# Synthesis and biological activity of pyridopyridazin-6-one p38 MAP kinase inhibitors. Part 1

Robert M. Tynebor [a,*], Meng-Hsin Chen [a], Swaminathan R. Natarajan [a], Edward A. O'Neill [b], James E. Thompson [b], Catherine E. Fitzgerald [b], Stephen J. O'Keefe [b], James B. Doherty [a]

[a] Department of Medicinal Chemistry, Merck Research Laboratories, PO Box 2000, Rahway, NJ 07065, USA
[b] Department of Inflammation Research, Merck Research Laboratories, PO Box 2000, Rahway, NJ 07065, USA

## ABSTRACT

The development and synthesis of potent p38α MAP kinase inhibitors containing a pyridazinone platform is described. Evolution of the p38α selective pyridopyridazin-6-one series from the p38α/β dual inhibitor 2H-quinolizin-2-one series will be discussed in full detail.

© 2010 Elsevier Ltd. All rights reserved.

Autoimmune driven diseases such as rheumatoid arthritis (RA), psoriatic arthritis, and inflammatory bowel disease can be treated by suppressing the activity of the proinflammatory cytokine tumor necrosis factor (TNF-α).[1] The monoclonal antibodies Infliximab (Remicade®), Adalimumab (Humira®), and the fusion protein Etanercept (Enbrel®) are currently used as effective treatment options.[2] An alternative therapeutic approach would be suppressing the production of TNFα with small molecule inhibitors designed to block the p38 mitogen-activated protein (MAP) kinase signal transduction cascade.[3] Although in vivo models indicate p38 is a viable therapeutic target to reduce symptoms of RA, no small molecule therapy has successfully reached the market.[2] This may be due to the fact that the majority of small molecule p38 inhibitors are only semi-selective, possessing minimal activity against p38δ and p38γ but binding equally well to p38α and p38β isoforms.[4] The difficulty in separating p38α and p38β inhibitory activity is a result of these isoforms having an ATP-inhibitor binding site that is 97% similar in sequence.[5] Recently it was reported that a dual p38α/β inhibitor could not suppress lipopolysaccharide (LPS) induced TNFα production in mice expressing T106 M modified p38α.[6] These results demonstrated p38β has no role in modulating TNFα levels and suggest that inhibition of this isoform would offer no positive therapeutic advantage in treating inflammation based diseases. Our research therefore focused on developing a selective

p38α inhibitor by modifying the previously disclosed quinolizin-2-one core (**1**)[7] (Fig. 1).

In 2000, the discovery of VX-745 (**2**) introduced a new class of heterobiaryl p38 inhibitors that possessed a high level of selectivity against a large spectrum of kinases.[8] This enhanced selectivity was a result of a novel structure-induced conformation or 'flip' of p38α/β Gly-110 and was critical in producing several structurally diverse second generation inhibitors.[9] VX-745 was also unique due to a moderate 18-fold selectivity for the p38α over the p38β isoform.[10]

Merck developed a novel class of p38α selective cyclic ureas represented by compound **3**.[11] Cyclic urea derivatives and **2** bind by using a carbonyl based B-ring to induce a Gly-110 'flip', occupying hydrophobic pocket 1 with a 2,6-dihalophenyl substituted A-ring, and occupying hydrophobic pocket 2 with a 2,4-dihalobenzenethiol C-ring (Fig. 2). Quinolizin-2-one **1** lacks the thio ether
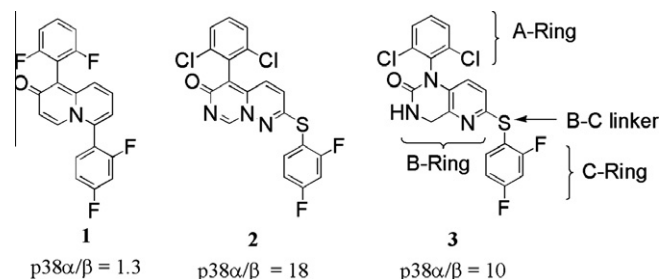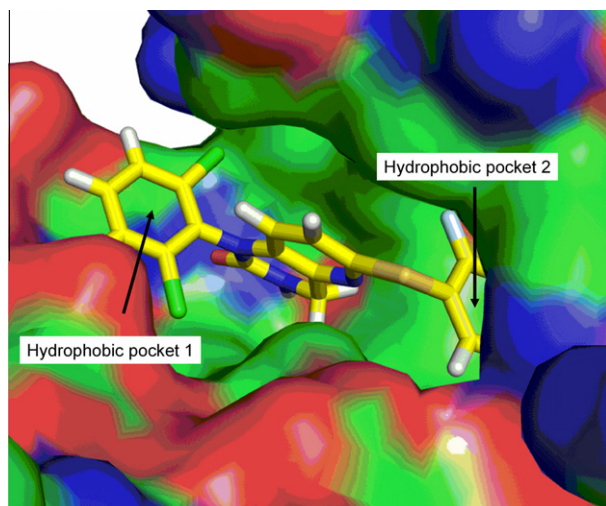
Figure 1. Isoform selectivity of quinolizin-2-one **1**, VX-745 (**2**), and urea **3**.
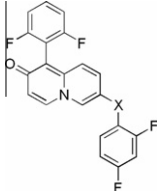
**Figure 2.** Molecular modeling image of compound **3** binding to the p38α active site.[13]

**Table 1**
p38α/β Activity of 7-substituted quinolizin-2-one derivatives



| Compound | X | p38α[12] IC$_{50}$ (nM) | p38β[12] IC$_{50}$ (nM) | α/β ratio |
|---|---|---|---|---|
| **1** | — | 7 | 9 | 1.3 |
| **4** | S | 320 | 3100 | 9.7 |
| **5** | O | 190 | 1530 | 8.1 |
| **6** | CH$_2$ | 93 | 1300 | 13.9 |
| **7** | NHCH$_2$ | 870 | 10,100 | 11.6 |
| **8** | C$_2$H$_2$ | 890 | 5900 | 6.6 |
| **9** | C$_2$H$_4$ | 490 | 6610 | 13.4 |

linker and as a result the 2,4 difluorophenyl C-ring is shifted over to the 6 position and therefore directly attached to the heterobiaryl core. This different B–C ring connectivity produces quinolizin-2-ones that only behave as dual p38α/β inhibitors. In both classes

of compounds the 2,4 difluoro aryl group occupy the same hydrophobic pocket and therefore selectivity may be a result of the different B–C ring connectivity.

In order to introduce selectivity into the quinolizin-2-one series a linker was installed at the 7 position and various attributes, such as length and composition were explored (Table 1). Single atom linkers **4–6** possessed moderate p38α activity and introduced an average of 10-fold selectivity. Elongation of the linker region to a methyl amine (**7**), ethyl (**8**), or ethylene (**9**) resulted in a substantial loss in p38α potency and offered no selectivity advantage over single atom linkers **4–6**.

Although our initial screening led to compounds with moderate p38α activity and enhanced selectivity, further changes to the molecule were necessary to increase potency and selectivity. Substituting the quinolizin-2-one core with a pyridopyridazin-6-one core reduces the calculated Log D and therefore may improve physical properties and functional activity.[14] Another advantage the pyridopyridazin-6-one core possessed is that **16** can serve as a valuable intermediate for future synthetic manipulations.

Synthesis of quinolizin-2-one derivatives **4–9** began with a Negishi coupling between 2,5-dibromopyridine and 2,6-difluorobenzylzinc bromide to yield diaryl methylene **11** (Scheme 1). LiHMDS generated the dibenzylic anion of **11** at −78 °C and was quenched with TMS propenyl ethyl ester to afford the protected diarylbutynone **12** in moderate yield. The TMS protecting group was removed and thermal cyclization generated the 2H-quinolizin-2-one platform **14**.[15] Compounds **4**, **5**, and **7** were synthesized using standard Ullmann procedures. Negishi coupling between **14** and 2,4-difluorobenzylzinc bromide yielded methylene linker **6**. Sonogashira coupling between bromide **14** and 1-ethynyl-2,4-difluorobenzene and subsequent alkyne hydrogenation using Lindlar's catalyst afforded alkene derivative **8**, while alkyne hydrogenation using 10% Pd/C yielded ethyl derivative **9**.

Pyridopyridazin-6-one analogs were synthesized using a similar synthetic protocol described in Scheme 1 (Scheme 2). After the 2-chloro pyridopyridazin-6-one **16** core was synthesized the chloride was readily displaced with various nucleophiles or coupled using synthetic protocols previously mentioned in Scheme 1 to yield analogs **17–61** (Tables 2–4).

Evaluating the B–C linker length of analogs **17–31** revealed a similar trend observed in the quinolizin-2-one series (Table 1) where potency dramatically decreased with an increase in linker length (Table 2). This trend is clearly observed when the B–C linker region was successively elongated from phenoxy **22** to phenylethoxy **23**. For each additional atom introduced into the linker region
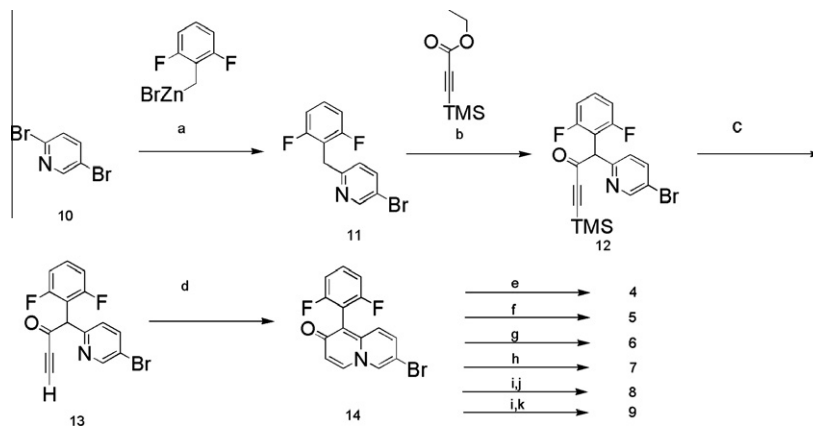


**Scheme 1.** Synthesis of quinolizin-2-ones **4–9**. Reagents and conditions: (a) Pd(PPh$_3$)$_4$, THF, reflux, 1 h, 46%; (b) LiHMDS, THF, −78 °C, 1 h, 51%; (c) TBAF, THF, 0 °C, 15 min, 60%; (d) TMEDA, 90 °C, 0.5 h, 50%; (e) 2,4-difluorophenol, 2,2,6,6-tetramethylheptane-3,5-dione, CuCl, Cs$_2$CO$_3$, NMP, 120 °C, 2 h, 62%; (f) 2,4-difluorobenzenethiol, 2,2,6,6-tetramethylheptane-3,5-dione, CuCl, Cs$_2$CO$_3$, NMP, 120 °C, 2 h, 68%; (g) bromo(2,4-difluorobenzyl)zinc, Pd(PPh$_3$)$_4$, THF, reflux, 1 h, 67%; (h) 1-(2,4-difluorophenyl)methanamine, 2,2,6,6-tetramethylheptane-3,5-dione, CuCl, Cs$_2$CO$_3$, NMP, 120 °C, 2 h, 34%; (i) 1-ethynyl-2,4-difluorobenzene, TEA, CuI, Pd(PPh$_3$)$_2$Cl$_2$, DMF, 100 °C, 4 h, 80%; (j) Lindlar catalyst, H$_2$, MeOH, 1 h, 55%; (k) Pd/C, H$_2$, MeOH, 1 h, 85%.
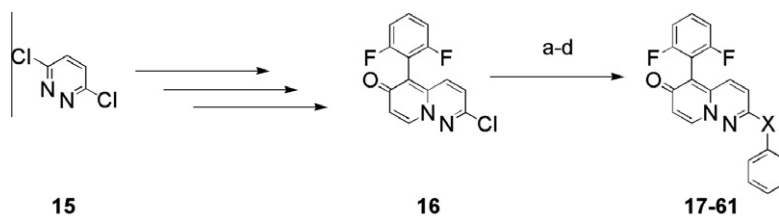
**Scheme 2.** Synthesis of pyridopyridazin-6-ones **17**–**61**. Reagents and conditions: (a) X = O; Cs$_2$CO$_3$, phenol, NMP, 90 °C, 2 h; (b) X = S; NaH, benzenethiol, THF, rt, 15 min; (c) X = CH$_2$; Pd(PPh$_3$)$_4$, benzyl zinc bromide, THF, 80 °C, 30 min; (d) X = N; tris(dibenzylideneacetone)dipalladium, 1,1′-bis(diphenylphosphino)ferrocene, sodium *t*-butoxide, aniline, toluene, 80 °C, 3 h.

**Table 2**
p38α Inhibitory activity of 2 substituted pyridopyridazin-6-one derivatives



| Compound | X | p38α[12] IC$_{50}$ (nM) | p38β[12] IC$_{50}$ (nM) | α/β | THP-1/TNFα[16] IC$_{50}$ (nM) | hWB/TNFα[12] IC$_{50}$ (nM) |
|---|---|---|---|---|---|---|
| 17 | | 3.2 | 33 | 10.3 | 17.9 | 29 |
| 18 | | 720 | >10,000 | — | N/A | N/A |
| 19 | | 4.7 | 86 | 18.3 | 29.0 | 26 |
| 20 | | >10,000 | >10,000 | — | N/A | N/A |
| 21 | | 1300 | >10,000 | — | N/A | N/A |
| 22 | | 160 | 1800 | 11.3 | 505 | N/A |
| 23 | | >10,000 | >10,000 | — | N/A | N/A |
| 24 | | 1300 | >10,000 | — | N/A | N/A |
| 25 | | 719 | >10,000 | — | N/A | N/A |
| 26 | | 3.5 | 45 | 12.8 | 16.3 | 64 |
| 27 | | 20 | 230 | 11.5 | 150 | 100 |
| 28 | | 650 | >10,000 | — | N/A | N/A |
| 29 | | 480 | 5500 | 11.4 | N/A | N/A |
| 30 | | 1430 | >10,000 | — | N/A | N/A |
| 31 | | 7.6 | 86 | 11.3 | 23.2 | 72 |

the potency decreased approximately 10-fold. The most selective compound in the two atom linker series was benzylamine **27** (11.5-fold) but failed to improve selectivity with respect to the quinolizin-2-one series.
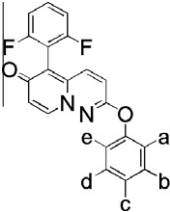
Oxygen linker **19** possessed p38α inhibitory activity 40-fold greater than similar quinolizin-2-one derivative **5** and improved p38α/β selectivity to 18-fold. Derivatives containing a thioether (**17**) or a methylene B–C linker (**31**) also dramatically increased potency with respect to quinolizin-2-ones **4** and **6**, but failed to improve selectivity. Since a dramatic shift in enzyme potency was observed between quinolizin-2-one **5** and pyridopyridazin-6-one **19**, both compounds were further investigated to understand the role of the additional nitrogen present in **19**.

Molecular modeling calculations minimized the rotational freedom associated with the ether linker and determined the energy difference between the lowest energy conformation of **5** and **19** was 1.3 kcal/mol.[13] As a result, the lowest energy conformation

of compound **5** positions the C-ring approximately 90° away from hydrophobic pocket 2, while compound **19** it positions the C-ring in a conformation more suitable to interact with hydrophobic pocket 2 (Fig. 3). This difference in low energy conformations may explain why the quinolizin-2-one series was significantly more potent than the pyridopyridazin-6-one series.

Due to the enhanced potency and selectivity of ether derivative **19**, the C-ring was further explored to determine the correlation between substitution and potency/selectivity in the pyridopyridazin-6-one series (Table 3). Fluoro and chloro substituted analogs drastically favored *ortho* or *para* substitution over the *meta* position. For example, 2-fluorophenyl **32** (12 nM) and 4-fluorophenyl **42** (48 nM) were 10–40 times more potent than 3-fluorophenyl **37** (420 nM), while 2-chlorophenyl **33** (44 nM), and 4-chlorophenyl **43** (79 nM) were 3–5 times more potent than 3-chlorophenyl **38** (240 nM). Methyl substituted derivatives followed a different trend in which the 2-methylphenyl (**34**, 92 nM) and

**Table 3**
p38α Inhibitory activity for mono substituted C-ring derivatives **32–46**



| Compound[a] | a | b | c | p38α[12] IC$_{50}$ (nM) | p38β[12] IC$_{50}$ (nM) | β/α | THP-1/TNFα[16] IC$_{50}$ (nM) | hWB/TNFα[12] IC$_{50}$ (nM) |
|---|---|---|---|---|---|---|---|---|
| **22** | — | — | — | 160 | 1800 | 11.3 | 505 | N/A |
| **32** | F | — | — | 12 | 180 | 15 | 67 | 171 |
| **33** | Cl | — | — | 44 | 360 | 8.2 | 102 | 352 |
| **34** | Me | — | — | 92 | 520 | 5.6 | 386 | N/A |
| **35** | OMe | — | — | 82 | 110 | 1.3 | 172 | 475 |
| **36** | CF$_3$ | — | — | 2400 | N/A | | N/A | N/A |
| **37** | — | F | — | 420 | 3700 | 8.8 | 977 | N/A |
| **38** | — | Cl | — | 240 | 2067 | 8.6 | 351 | N/A |
| **39** | — | Me | — | 70 | 660 | 9.4 | 376 | N/A |
| **40** | — | OMe | — | >10,000 | N/A | | N/A | N/A |
| **41** | — | CF$_3$ | — | >10,000 | N/A | | N/A | N/A |
| **42** | — | — | F | 48 | 1400 | 29 | 160 | N/A |
| **43** | — | — | Cl | 79 | 1900 | 24 | 170 | N/A |
| **44** | — | — | Me | 260 | 1900 | 7.3 | N/A | N/A |
| **45** | — | — | OMe | >10,000 | N/A | | N/A | N/A |
| **46** | — | — | CF$_3$ | >10,000 | N/A | | N/A | N/A |

[a] d = e = H for **22** and **32–46**.

**Table 4**
p38α Activity for substituted C-ring derivatives

| Compound | a | b | c | d | e | p38α[12] IC$_{50}$ (nM) | p38β[12] IC$_{50}$ (nM) | β/α | THP-1/TNFα[16] IC$_{50}$ (nM) | hWB/TNFα[12] IC$_{50}$ (nM) |
|---|---|---|---|---|---|---|---|---|---|---|
| **22** | — | — | — | — | — | 160 | 1800 | 11.3 | 505 | 480 |
| **47** | F | F | — | — | — | 32 | 300 | 9.4 | 97 | 392 |
| **48** | Cl | Cl | — | — | — | 32 | 220 | 6.8 | 61 | 689 |
| **19** | F | — | F | — | — | 4.7 | 86 | 18.3 | 29 | 26 |
| **49** | F | — | Cl | — | — | 11 | 180 | 16.3 | 27 | 75 |
| **50** | Cl | — | F | — | — | 14 | 130 | 9.3 | 52 | 154 |
| **51** | Cl | — | Cl | — | — | 30 | 220 | 7.3 | 57 | 552 |
| **52** | F | — | — | F | — | 130 | 1700 | 13.1 | 92 | 265 |
| **53** | Cl | — | — | Cl | — | 280 | 1400 | 5.0 | >10,000 | >10,000 |
| **54** | F | — | — | — | F | 95 | 1200 | 12.6 | 295 | >10,000 |
| **55** | Cl | — | — | — | Cl | 90 | 610 | 6.8 | 183 | 183 |
| **56** | F | — | F | — | F | 200 | 2400 | 12.0 | 115 | 462 |
| **57** | Cl | — | F | — | Cl | 68 | 310 | 4.6 | 58 | 453 |
| **58** | F | F | F | F | F | 4300 | >10,000 | — | >10,000 | >10,000 |
| **59** | — | F | F | — | — | 270 | 3300 | 12.3 | >10,000 | >10,000 |
| **60** | — | Cl | F | — | — | 140 | 1200 | 8.6 | >10,000 | >10,000 |
| **61** | — | Cl | Cl | — | — | 260 | 2700 | 10.4 | >10,000 | >10,000 |
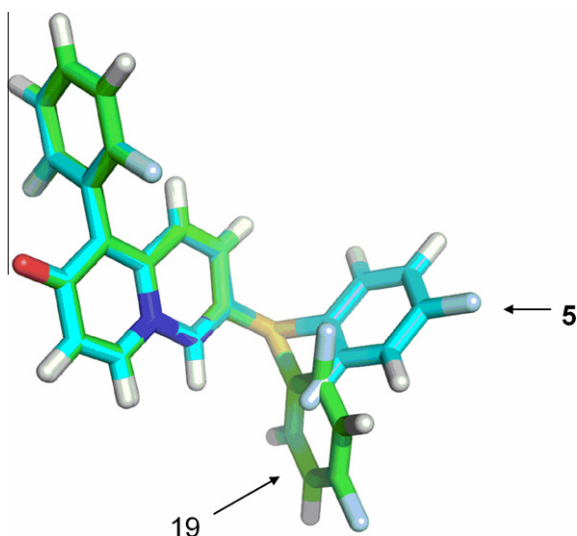
**Figure 3.** Lowest energy conformation for compounds **5** and **19**.

**Table 5**
Pharmacokinetic properties of compounds **17**, **19**, and **31**

| Compound[a,b] | $t_{1/2}$ (h) | Cl (mL/min/kg) | AUC (µM h) | F (%) |
|---|---|---|---|---|
| **17**[c] | 0.9 | 37.9 | 0.33 | 30 |
| **19**[d] | 1.1 | 11.6 | 3.6 | 96 |
| **31**[d] | 6.5 | 1.8 | 26.8 | 71 |

[a] IV dose = 1.0 mg/kg.
[b] PO dose = 2.0 mg/kg.
[c] PO vehicle = PEG-200/DMSO/water 70:10:20 (v/v/v).
[d] PO vehicle = PEG-200/water 70:30 (v/v).

**Table 6**
Reduction of TNFα levels in rat LPS induced arthritic model at 4 and 24 h

| Compound[a] | 4 h (%) | 24 h (%) |
|---|---|---|
| **19** | 30 | 0 |
| **31** | 75 | 55 |

[a] 3 mg/kg PO dose.

3-methylphenyl (**39**, 70 nM) derivatives possessed similar potency and were 3–4-fold more potent than 4-methylphenyl **44** (260 nM). Analogs bearing the larger methoxy or trifluoromethyl groups exhibited a large drop in activity regardless of substituent position. Selectivity was enhanced with respect to the unsubstituted phenyl **22** only when a 2-fluorophenyl (**32**), 4-fluorophenyl (**42**), or 4-chlorophenyl (**43**) were present. The 4-fluorophenyl analog (**42**) possessed the highest p38α/β selectivity ratio (29-fold) and was approximately threefold more selective than **22**.

Multi substituted C-ring analogs followed a potency and selectivity trend similar to that observed in the mono substituted series (Table 4). *ortho* and *para* Substituted analogs consistently yielded the highest potency when compared with other substitution patterns. The addition of a 2 fluoro substituent to a 3 or 4 substituted phenyl group improved potency approximately 10-fold for analogs **19**, **47**, and **49**. A similar increase in potency was also observed when a chlorine was added to the 2 position, but the potency shift was less dramatic than analogous 2 fluoro analogs. Fluorines were critical for p38α binding potency and significantly improved whole blood data when compared to chlorines. This trend in functional potency was due to the increased hydrophobicity of the chloro derivatives and their effects on physical properties. However, addi-

tional fluoro substituted derivatives such as trifluorophenyl **56** and pentafluoro **58** derivatives failed to improve potency with respect to the bis fluoro derivative **19**.

Although disubstituted C-ring analogs yielded enhanced binding potency when compared to monosubstituted derivatives, selectivity failed to improve. For example, 2,4-difluorophenyl analog **19** was 10-fold more potent than **42**, but less selective. A similar trend was also observed between 4-chlorophenyl analog (**43**) and 2,4-dichlorophenyl analog (**51**).

SAR of the C-ring indicated that only small hydrophobic groups were tolerated at the 2 and 4 positions. Molecular modeling of **3** in the p38α crystal structure shows the small size of hydrophobic pocket 2 suggesting an explanation for the SAR potency trend we observed (Fig. 4).[13] However, the overlapping crystal structure of **3** in p38α and p38β failed to suggest an explanation for the selectivity trend. The residues that comprise hydrophobic pocket 2 are identical for p38α and p38β and very little movement is observed when **3** binds. The only residue which moved significantly was D168, but C-ring substitution in this region failed to improve selectivity. This would imply that modifications in the B–C linker and C-ring region only affect selectivity by causing other parts of the molecule to shift in the binding site with respect to dual inhibitors. This hypothesis will be communicated in a separate manuscript.
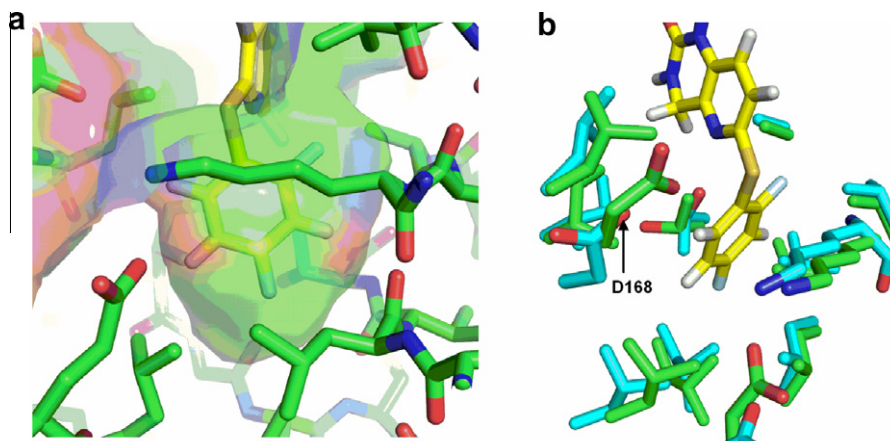


**Figure 4.** Model of **3** occupying hydrophobic pocket 2 (a) and **3** binding to superimposed p38α and p38β enzymes (b).
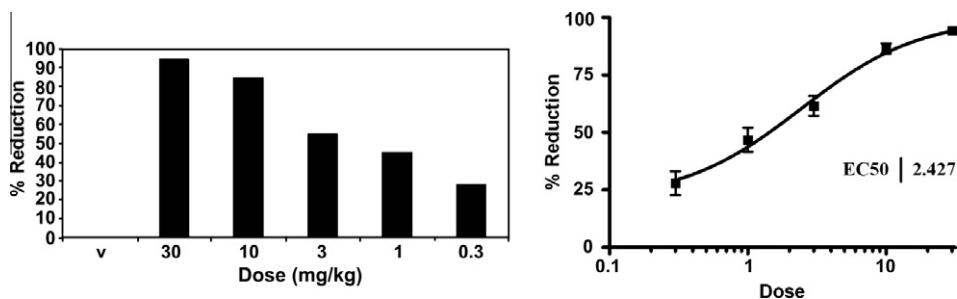
**Figure 5.** Calculated $EC_{50}$ of **31** at 24 h in the LPS induced TNFα rodent model.

Compounds **17**, **19**, and **31** possessed the best balance between functional activity and selectivity and were further evaluated to determine pharmacokinetic properties (Table 5). Composition of the linker region played a major role in determining the pharmacokinetic profile of pyridopyridazin-6-one derivatives. Oxygen derivative **19** significantly increased the AUC and bioavailability when compared to the historical thioether linker of **17**. Methylene linker **31** further improved the pharmacokinetic profile of **19** by increasing the AUC an additional 10-fold, lowering clearance to 1.8 mL/min/kg, and increasing $t_{1/2}$ to 6.5 h.

Compounds **19** and **31** were evaluated in the LPS induced arthritic rodent model to assess their ability to decrease high levels of TNFα at 4 and 24 h (Table 6). A 3 mg/kg dose of **31** reduced TNFα levels by 75% while **19** only reduced levels by 30% after 4 h. At the 24 h time point **19** showed no apparent reduction in TNFα levels while **31** reduced levels by 55% with respect to the vehicle. Additional doses of **31** were tested to determine that the effective concentration needed to reduce TNFα by 50% ($EC_{50}$) at the 24 h time point was 2.4 mg/kg (Fig. 5). Although both compounds have similar functional activity, the superior pharmacokinetic properties of **31** resulted in a higher degree of efficacy in the LPS rodent model.

Our efforts led to the discovery of a novel class of pyridopyridazin-6-one derived p38α inhibitors that possessed moderate p38α/β selectivity, excellent functional activity, and efficacy in the rat LPs model. The process of transforming a p38α/β dual inhibitor into a p38α selective inhibitor identified several important structural traits necessary to balance selectivity and potency. The end result of this research was the development of a structurally unique series that could serve as a template for further optimization.

## Acknowledgment

## References and notes

1. (a) Palladino, M. A.; Bahjat, F. R.; Theodorakis, E. A.; Moldawer, L. L. *Nat. Rev. Drug Disc.* **2003**, *2*, 736; (b) Saklatvala, J. *Curr. Opin. Pharmacol.* **2004**, *4*, 372.
2. Stoll, J. G.; Yasothan, U. *Nat. Rev. Drug Disc.* **2009**, *8*, 693.
3. (a) Kumar, S.; Boehm, J.; Lee, J. C. *Nat. Rev. Drug Disc.* **2003**, *2*, 717; (b) Pettus, L. H.; Wurz, R. P. *Curr. Top. Med. Chem.* **2008**, *8*, 1452.
4. (a) Hynes, J.; Leftheris, K. *Curr. Top. Med. Chem.* **2005**, *5*, 967; (b) Goldstein, D. M.; Kuglstatter, A.; Lou, Y.; Soth, M. J. *J. Med. Chem.* **2010**, *53*, 2345.
5. Patel, S. P.; Cameron, P. M.; O'Keefe, S. J.; Frantz-Wattley, B.; Thompson, J. B.; O'Neill, E. A.; Tennis, T.; Liu, L.; Becker, J. W.; Scapin, G. *Acta Crystallogr., Sect. D* **2009**, *65*, 777.
6. O'Keefe, S. J.; Mudgett, J. S.; Cupo, S.; Parsons, J. N.; Chartrain, N. A.; Fitzgerald, C.; Chen, S.-L.; Lowitz, K.; Rasa, C.; Visco, D.; Luell, S.; Carballo-Jane, E.; Owens, K.; Zaller, D. M. *J. Biol. Chem.* **2007**, *282*, 34663.
7. Tynebor, R. M.; Chen, M.-H.; Natarajan, S. R.; O'Neill, E. A.; Thompson, J. E.; Fitzgerald, C. E.; O'Keefe, S. J.; Doherty, J. B. *Bioorg. Med. Chem. Lett.* **2010**, *20*, 2765.
8. (a) Bemis, G. W.; Salituro, F. G.; Duffy, J. P.; Harrington, E. M. U.S. Patent 6147,080, 2000; (b) Salituro, F.; Bemis, G.; Cochran, J. WO 99/64,400.
9. (a) Natarajan, R. S.; Doherty, J. B. *Curr. Top. Med. Chem.* **2005**, *5*, 987; (b) Herberich, B.; Cao, G.-Q.; Chakrabarti, P. P.; Falsey, J. R.; Pettus, L.; Rzasa, R. M.; Reed, A. B.; Reichelt, A.; Sham, K.; Thaman, M.; Wurz, R. P.; Xu, S.; Zhang, D.; Hsieh, F.; Lee, M. R.; Syed, R.; Li, V.; Grosfeld, D.; Plant, M. H.; Henkle, B.; Sherman, L.; Middleton, S.; Wong, L. M.; Tasker, A. S. *J. Med. Chem.* **2008**, *51*, 6271.
10. In house data.
11. Liu, L.; Stelmach, J. E.; Natarajan, S. R.; Chen, M. H.; Singh, S. B.; Schwartz, C. D.; Fitzgerald, C. E.; O'Keefe, S. J.; Zaller, D. M.; Schmatz, D. M.; Doherty, J. B. *Bioorg. Med. Chem. Lett.* **2003**, *13*, 3979.
12. (a) Liverton, N. J.; Butcher, J. W.; Claiborne, C. F.; Claremon, D. A.; Libby, B. E.; Ngyuen, K. T.; Pitzenberger, S. M.; Selnick, H. G.; Smith, G. R.; Tebben, A.; Vacca, J. P.; Varga, S. L.; Agarwal, L.; Dancheck, K.; Forsyth, A. J.; Fletcher, D. S.; Frantz, B.; Hanlon, W. A.; Harper, C. F.; Hofsess, S. J.; Kostura, M.; Lin, J.; Luell, S.; O'Neill, E. A.; Orevillo, C. J.; Pang, M.; Parsons, J.; Rolando, A.; Sahly, Y.; Visco, D. M.; O'Keefe, S. J. *J. Med. Chem.* **1999**, *42*, 2180; (b) A SPA-bead based assay was carried out using mouse p38. Compounds were serially diluted into a 96 well plate containing a MOPS based p38 assay buffer. The assay was initiated by addition of cold ATP, $^{33}$P ATP (gamma) and biotin labeled GST-ATF2 substrate (4 μM). After incubation at 30 °C for 3 h, the reaction was stopped by addition of a PBS based quench buffer with 2× moles of SPA beads over the amount of substrate used. The extent of phosphorylation of GST-ATF2 was measured using a top count reader and subtracted from background. $IC_{50}$s are means of two experiments.
13. Computed using the mixed torsional/low-mode sampling algorithm as implemented in Maestro v 9.02 from the software company, Schrodinger. Used the MMFFs force field in the gas phase with a distance dielectric constant of 2.
14. Calculated Log *D* values: **5** = 6.08 ± 0.88, **19** = 4.53 ± 0.90. ACDLabs 11.0.
15. Natarajan, S. R.; Chen, M.-H.; Heller, S. T.; Tynebor, R. M.; Crawford, E. M.; Minxiang, C.; Kaizheng, H.; Dong, J.; Hu, B.; Hao, W.; Chen, S.-H. *Tetrahedron Lett.* **2006**, *47*, 5063.
16. Anti human TNF-α was coated on immulon 4 plates. THP-1 cells (density = 2.5 × 10⁶/mL) were suspended into 96-well plates containing a PBS based medium. Compound was added as solution in DMSO followed by addition of LPS. The reaction was incubated for 4 h at 37 °C under $CO_2$. TNFα release was measured in the supernatants by ELISA. Reported $IC_{50}$s are means from three measurements.